Application of melon seed shell as a natural low-cost adsorbent for the removal of Methylene Blue from dye-bearing wastewaters: optimization, isotherm, kinetic, and thermodynamic

Mehdi Rahimdokht, Elmira Pajootan*, Mokhtar Arami

Textile Engineering Department, Amirkabir University of Technology, 424 Hafez Ave, Tehran, Iran,
email: Mehdi.rahimdokht@gmail.com (M. Rahimdokht), Tel. +98 2164542681; Fax: +98 2166400245; emails: pajootan@aut.ac.ir
(E. Pajootan), arami@aut.ac.ir (M. Arami)

ABSTRACT

In this study, melon seed shells (MSS) were employed for the removal of hazardous methylene blue (MB) from the simulated wastewaters by the adsorption process. Fourier transform infrared spectra, field emission scanning electron microscope images, isoelectric pH (pH_{ZPC}), X-ray diffraction, and BET analysis were used to characterize the MSS biosorbent. The adsorption processes were conducted by changing the initial dye concentration, MSS dosage, pH of the solution, time, temperature, and the inorganic salts concentration as selective parameters that affect the removal efficiency. The results indicated that MB (30 mg/L) can be effectively removed (91.62%) at pH 7 and MSS dosage of 1.5 g/L after 150 min. The isotherm and kinetic parameters were also investigated, and the adsorption data were best fitted to the Temkin isotherm and pseudo-first-order kinetic model. The study of thermodynamic parameters by varying the solution temperature illustrated the endothermic and spontaneous nature of the adsorption process. The regeneration and desorption studies demonstrated the reusability of MSS for six cycles of adsorption and desorption with approximately 92% of dye removal. The overall obtained results can suggest MSS as a natural and low-cost adsorbent for the removal of cationic dyes such as MB from the contaminated effluents.

Keywords: Melon seed shell (MSS); Low-cost adsorbent; Methylene blue; Isotherm; Kinetic; Thermodynamic

1. Introduction

Water contamination caused by pollutants of different varieties, which are discharged into the water sources by means of industrial activities is one of the fundamental environmental problems. Moreover, organic dye molecules are considered as one of the main water pollutants, which are frequently found in industrial wastewaters such as textile, paper, leather, plastics, cosmetics, and food [1–3]. The discharge of untreated colored wastewaters into the environment can cause serious health problems to human, plants, and animals other than their esthetic impact, owing to their high visibility in trace amount [4,5].

Among the various reported methods available for the wastewater treatment such as filtration, biological

*Corresponding author.

treatment, coagulation, and advanced oxidation processes, the adsorption processes are being extensively applied to conquer the environmental hazards of organic compounds, especially dye molecules [6]. Adsorption process is known as the adherence of organic pollutants onto the surface of solids through the physical or chemical forces [7,8]. The main reasons for the superiority of adsorption process to the other procedures are: low-cost, simplicity of design, facility of process, high efficiency, availability of adsorbent, and ability for the separation of wide range of chemicals [9]. In order to benefit from these advantages of adsorption process, natural and low-cost biosorbents are being extensively investigated by researchers around the world. Several biosorbents, industrial and agricultural wastes, and natural adsorbents such as rice husk, coconut shell, waste carbon slurries, metal hydroxide sludge, and fish bone have been used for the removal of organic and inorganic pollutants from effluents [9–12].

To develop a new low-cost approach toward the efficient and effective removal of MB from dye-containing solutions, melon seed shell (MSS) was prepared to be employed as a natural adsorbent. Melon is a widely consumed fruit of Cucurbitaceae family, of which there are numerous varieties. However, the seeds of this fruit are not much consumed and they are thrown away, which might be considered as an economical and nutritional loss [13,14]. Melon seeds can be classified as agro-industrial wastes (byproduct) without any reports heard about their commercial and/or industrial application; however, they may be oxidized after being discharged into landfills and water bodies to cause serious environmental problems [15,16]. Although, Gill et al. reported that the melon seeds have therapeutic (anti-inflammatory and analgesic) effects as antioxidant, but they are usually discarded as an agricultural waste [16,17].

The surface morphology and functional groups existing in the structure of the prepared MSS were characterized by field emission scanning electron microscope (FESEM) images and Fourier transform infrared (FTIR) analysis. The isoelectric pH (pH$_{zpc}$, pH of zero point charge) of MSS was also determined to evaluate the surface charge of the adsorbent in the solution containing different values of pH. Moreover, the specific surface area and crystalline structure of MSS were studied using BET and X-ray diffraction (XRD) analyses. The important parameters affecting the removal efficiency including pH, initial MB concentration, adsorbent dosage, inorganic salt, and temperature were investigated to achieve the optimum condition for MB removal. Desorption of MB molecules at various pH values and the regeneration of MSS for seven cycles of adsorption and desorption was also examined. The equilibrium parameters such as adsorption isotherms (Langmuir, Freundlich, and Temkin), kinetics (pseudo-first-order, pseudo-second-order, and intra-particle diffusion models), and thermodynamics (free Gibbs energy, enthalpy, and entropy) were surveyed to recognize the mechanism of the adsorption, the rate of the removal process, and to know the nature of the adsorption to be either endothermic or exothermic.

2. Materials and methods

2.1. Preparation of MSS

The melon seeds and other waste materials were first removed from the melon fruit, of which 32.15% were the seeds. The waste materials were washed away with water and separated from melon seeds. The separated seeds contain water (37.15%), seed kernel (39.36%), and seed shell (23.49%). Then, the seeds were milled with a mortar, the inner part of the seed (seed kernel) was separated, and the seed shells were dried in oven at 50°C. Then, they were sieved to particle sizes ranged from 250 to 400 μm and finally washed with distilled water for three times. The prepared adsorbent was dried in oven at 50°C for 10 h.

2.2. Adsorption procedure

C.I. Basic Blue 9 (methylene blue (MB), $C_{16}H_{18}ClN_3S$, and 319.85 g/mol) was supplied by Ciba Ltd. Other chemicals were of analytical grade, and they were purchased from Merck. The synthetic dye solutions were prepared by adding a specific amount of MB aqueous solution to distilled water, and the pH of the solutions was adjusted to the desirable value using H_2SO_4 (0.1 M) or NaOH (0.1 M).

Batch adsorption experiments were conducted on a magnetic stirrer with the constant stirring rate of 200 rpm. The adsorption process was carried out by the addition of various dosages of MSS (0.5, 1.0, 1.5, and 2.0 g/L) to 250 mL of dye solution (10, 20, 30, 40, 50, and 60 mg/L) at different pH values (3.0, 5.0, 7.0, 9.0, and 11.0) for 150 min at 30 ± 1°C. The samples were taken from the solution at various time intervals (0, 5, 10, 15, 20, 30, 40, 50, 60, 80, 100, 120, and 150 min), they were centrifuged by Hettich EBA20 at 5,000 rpm for 10 min, and their absorbance was measured at time = 0 (A_0) and after the time = t (A) using a Vis spectrophotometer (Unico2100, China) at the maximum wavelength (λ_{max} = 665 nm). The MB removal efficiency was calculated using Eq. (1) [18]:

$$\text{MB removal efficiency} (\%) = \left(\frac{A_0 - A}{A_0}\right) \times 100 \quad (1)$$

The amount of dye per unit mass of MSS is calculated employing the Eq. (2):

$$q = \frac{(C_0 - C_e)V}{m} \quad (2)$$

where C_0 and C_e are the initial and equilibrium dye concentrations (mg/L), m is the mass of adsorbent (g), and V is the volume of solution (L) [18].

2.3. Desorption studies

First, MSS was employed to remove 30 mg/L of MB (the optimum initial MB concentration for dye removal) at pH 7 for 250 min. Next, the dye-loaded MSS was separated from solution and dried at 30°C for 12 h. Then, 0.8 g/L of MB-loaded MSS was added to 250 mL of distilled water at various pH values (3–11) at 30 ± 1°C. The fraction of dye molecules desorbed from MSS is calculated using the following equation [19]:

$$\text{Desorption} (\%) = \left(\frac{\text{Amount released to solution}\left(\frac{\text{mg}}{\text{L}}\right)}{\text{Total adsorbed} \ \left(\frac{\text{mg}}{\text{L}}\right)}\right) \times 100 \quad (3)$$

2.4. Methods of characterization

The FTIR spectroscopy of the MSS before and after the dye adsorption was measured with a Thermo Nicolet Avatar 360 FTIR spectrometer within the range of 500–4,000 cm^{-1} to identify the surface functional groups of MSS and the variation of spectra after the adsorption process.

The surface morphology of MSS before and after the adsorption of MB was examined using a FESEM (JSM-6700F, JEOL, Japan).

The isoelectric pH (pH$_{\text{ZPC}}$) of the MSS adsorbent was determined by the addition of MSS (1 g) to 50 mL of KNO$_3$ solution (0.01 M). The initial pH of solutions was adjusted from 2.0 to 11.0 using HNO$_3$ and NaOH. The solutions were stirred for 24 h and the final pH was recorded. The pH in which the value (ΔpH = pH$_i$ − pH$_f$) equals zero is known as pH$_{\text{ZPC}}$ [20].

The specific surface area of MSS was evaluated by N$_2$ adsorption at 77 K with the relative pressure in the range of 0.01–0.4 using Belsorp-mini II Bel, Japan. The total pore volume (the volume of liquid nitrogen corresponding to the adsorbed amount) of the sample was measured at a $P/P_0 = 0.990$. The pore size distributions were deduced using the Barrett–Joyner–Halenda (BJH) method. Before measurements, the sample was put in a vacuum oven at 40°C for 24 h.

XRD pattern of MSS was obtained by X-ray diffractometer (EQuinox 3000) using Cu Kα radiation. The data were recorded over a 2θ range of −10–119° with a step size of 0.03°.

3. Results and discussion

3.1. Characterization of MSS

An adsorption process is initiated by the electrostatic interaction between the adsorbent and adsorbate. The pH$_{\text{ZPC}}$ of MSS was investigated to determine its surface charge at different media to provide the best condition for the removal of MB from aqueous solution. Fig. 1 shows pH$_{\text{ZPC}}$ of MSS indicating that the pH at which the overall surface charge of MSS equals zero is 5.5. As a result, the surface of MSS is positively charged at pH < 5.5 via protonation of its functional groups by the dominant H$^+$ existing in the solution. In contrast, high amounts of HO$^-$ groups at pH values higher than 5.5 make the MSS surface negatively charged. According to these results, high pH values favor the adsorption of cationic MB molecules via negatively charged MSS by the domination of electrostatic attraction forces.

The XRD pattern of MSS is also shown in Fig. 1. The results show the most intense peaks at 2θ of 16.12° and 22.03° for (1 1 0) and (2 0 0), and the peak at 34.75° is related to (0 0 4), which reflect the characteristic of polymorph of cellulose type I. This result confirms the cellulosic nature of MSS [21].

In Fig. 2, the FTIR spectra of MSS, MB, and MSS after the adsorption of MB (MSS–MB) are presented. The broad peak at 3,427 cm^{-1} in MSS is attributed to the O–H stretching bond existing in its structure or due to water absorption in the atmosphere. The sharper peak at 3,438 cm^{-1} in MB sample is due to the N–H stretching bond. The peaks at 2,922 and 2,855 cm^{-1} in all samples are related to the symmetric alkane stretching of C–H bond. The peaks at 1,486 and 1,592 cm^{-1} are related to the aromatic C=C stretching bond in MB. The peak appearing at 1,243 cm^{-1} is probably attributed to the C–N amine in MB. Peaks at 820 and 880, 1,386, and 1,000–1,220 cm^{-1} are corresponding to the bending vibrations of the C–H groups of the heterocycle, bending vibrations of the unsaturated dimethylamino groups and skeletal vibrations of the heterocycle of MB, respectively.
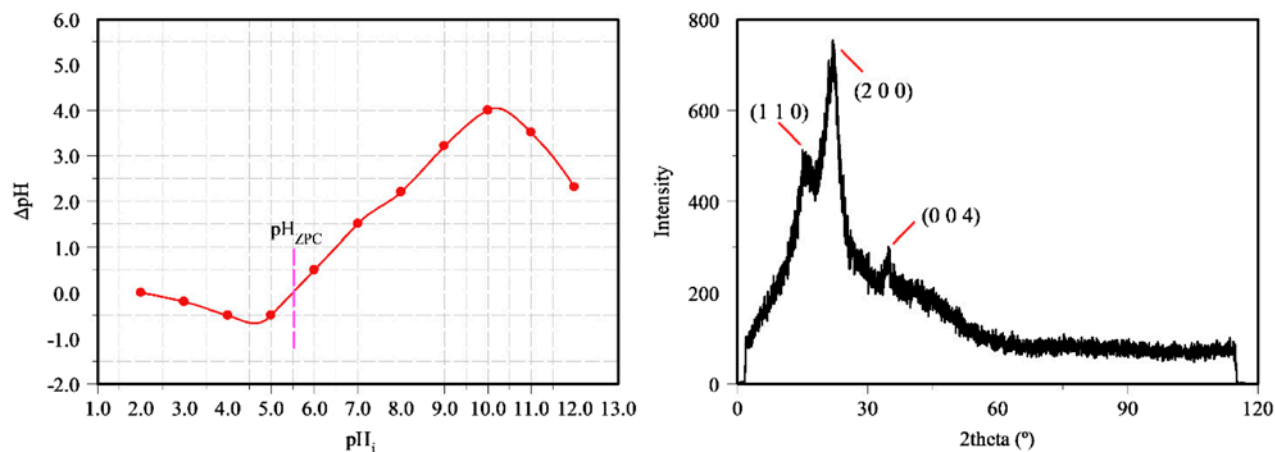
Fig. 1. pH$_{ZPC}$ and XRD patterns of MSS.
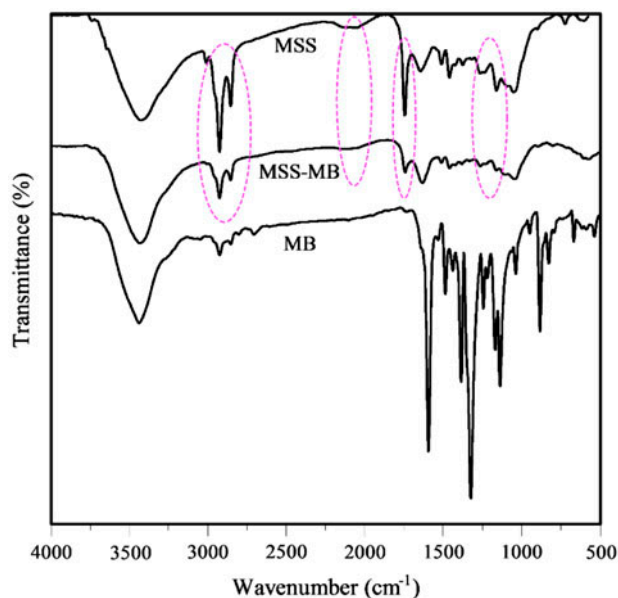
Fig. 2. FTIR spectra of MSS before and after the adsorption of MB.

The peak observed at 1,744 cm^{-1} can be attributed to the C=O ester bond in the structure of MSS. The peaks assigned to C=C and C≡C in MSS appeared at 1,644 and 2,062 cm^{-1}, respectively. The peaks at 1,263 and 1,161 cm^{-1} could be due to the stretching and bending vibrations of C–O groups in MSS. The weak peak at 723 cm^{-1} can also be related to the long chain band in the structure of MSS. The decrease in the intensity of several peaks at 2,922, 2,855, 2,062, 1,744, 1,263, and 1,161 cm^{-1} corresponding to the alkane, alkyne, carboxyl, and carbonyl groups can be ascribed to the involvement of their assigned bonds in the adsorption of MB [9,22].

The surface morphology of MSS was investigated by FESEM images at various magnifications (Fig. 3). The two observed constructions of MSS can be related to the different structure of the front and back sides of MSS, however, in both of these images, MSS has shown a relatively porous structure, which is one of the main characteristics of MSS other than its surface charge to be suitable for the adsorption process.

The results of BET indicated that the specific surface area of MSS was 3.0424 m^2/g and the total pore volume and average pore diameter were 0.028849 cm^3/g and 37.93 nm, respectively. These results are adequate for the adsorption of dye molecules from aqueous solutions [21].

3.2. Adsorption process

3.2.1. Effect of pH

The effect of pH on dye removal efficiency was investigated in the range of 3.0–11.0. Changing the pH of solution will vary the surface charge of the adsorbent and, therefore, will influence the dye removal efficiency. The results of pH variation are shown in Fig. 4. According to the experimental data, the dye removal efficiencies increased from 5.76 to 91.62% by increasing the pH values from 3.0 to 7.0. At low pH values (below the isoelectric pH), the surface of MSS is positively charged; and because of the strong repulsion forces between the positive adsorption sites of MSS and cationic MB molecules, low removal efficiencies are achieved. On the other hand, the reason of high removal percentages at alkali media can be explained by the deprotonation of adsorbent when the pH value is increased. According to the obtained results from pH$_{ZPC}$, the surface of MSS is negatively
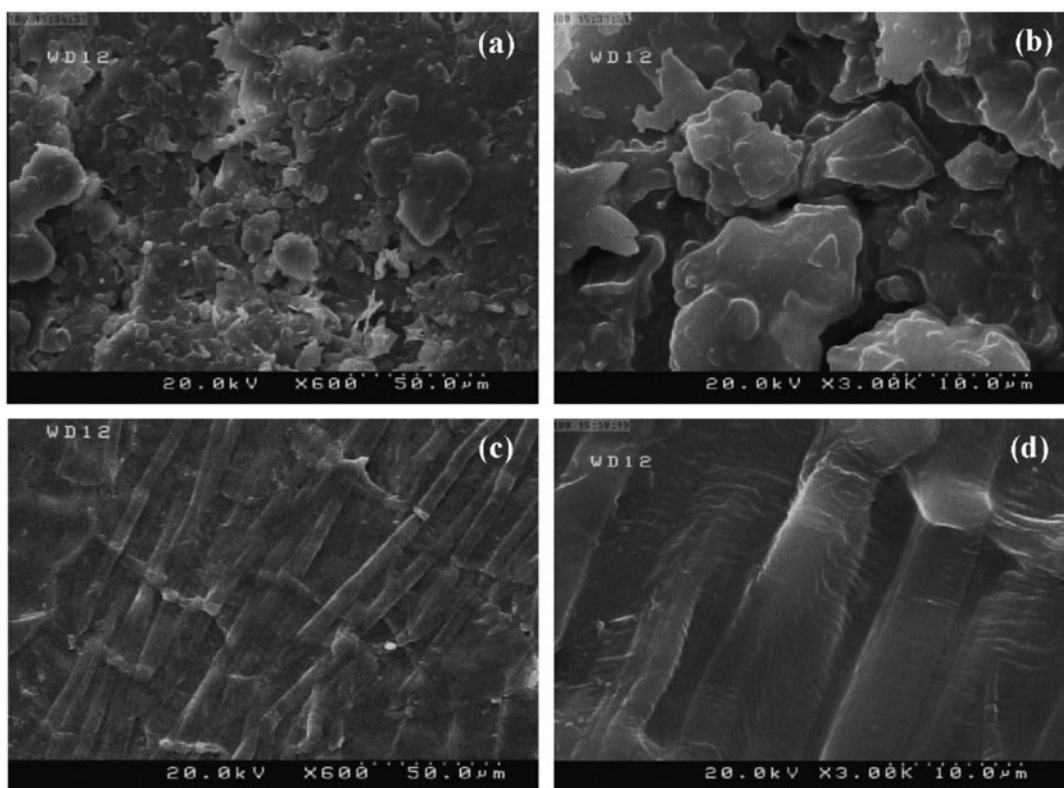
Fig. 3. FESEM images of the surface of MSS at different magnifications.
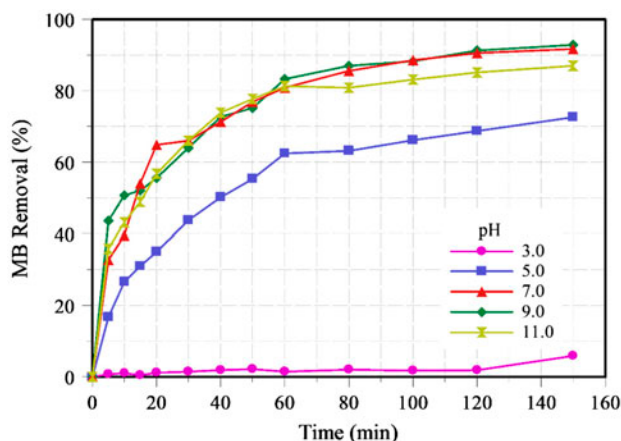
Fig. 4. Effect of pH on MB removal (%) ([MB_0]: 30 mg/L, MSS dosage: 1.5 g/L, and T: 30℃).

charged at pH > 5.5, which means that O–H, C=O, and C–O functional groups are negatively charged owing to the adsorption of OH⁻, thus the adsorption of MB in such media is probably due to the electrostatic attraction forces between the positively charged dye molecules and MSS negative functional groups [20]. Moreover, a scheme illustrating the functional groups of MSS involved in the adsorption of MB is presented in Fig. 5. Electrostatic attraction between the negative C=O and C–O functional groups in alkali media and positively charged MB molecules, van der Waals interaction between C–H groups of MSS and MB, and also, the π–π interaction between the MSS alkyne groups and aromatic rings in the structure of MB can be the responsible forces in the adsorption process of MB by MSS, which was approved by FTIR analysis [23]. Further increasing of pH value did not increase the MB removal efficiencies noticeably, thus, pH 7 was chosen as the optimum value for the adsorption process.

3.2.2. Effect of MSS particle size and dosage

The MSS dosage from 0.5 to 2.0 g/L was added to the colored solution to survey its effect on the adsorption behavior of MSS. The results shown in Fig. 6 illustrated that increasing the dosage of MSS up to 1.5 g/L will increase the removal (%) up to 91.62% because of the more available adsorption sites on the surface of adsorbent for the removal of dye molecules from the bulk solution. The addition of 2.0 g/L of MSS leads to the efficiency of 92.39%, which showed
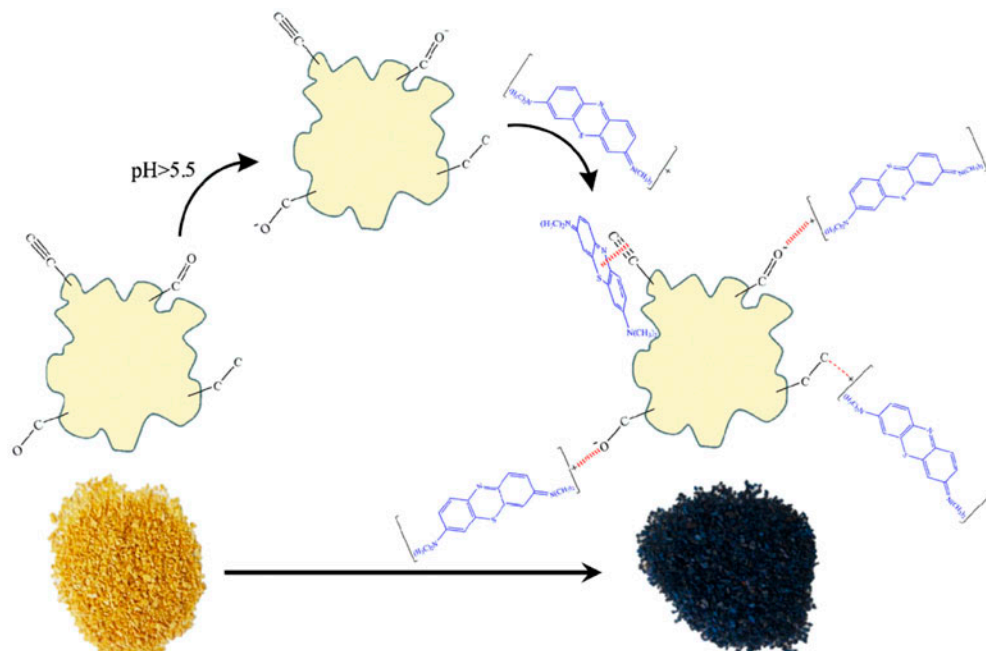
Fig. 5. Adsorption mechanism of MB by MSS.
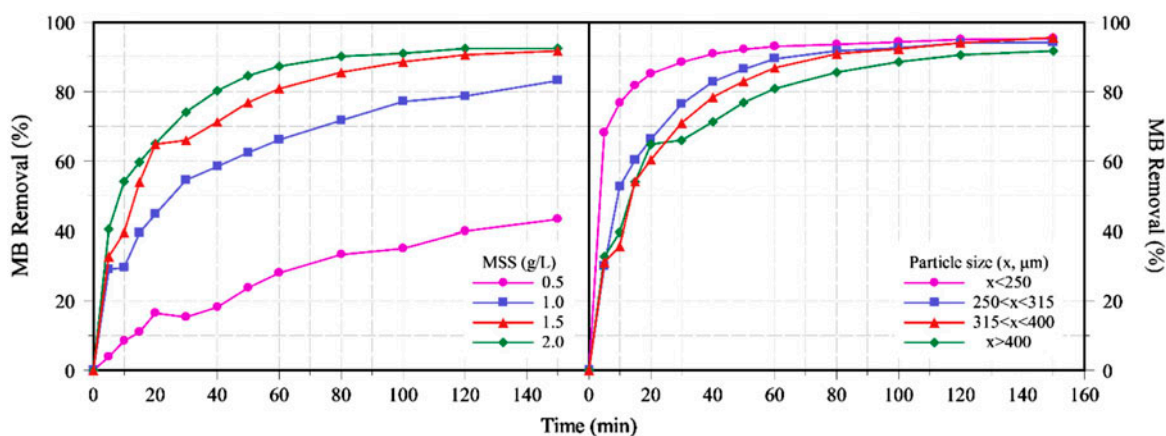
Fig. 6. Effect of MSS dosage and particle size on MB removal (%) ([MB_0]: 30 mg/L, pH 7.0, and T: 30℃).

only a negligible increase in the performance of the adsorption process. As it can be seen in Fig. 6, the adsorption process at initial times of the process was fast, but it became slow after about 90 min. This can be explained by the occupation of adsorption sites on MSS and the repulsion forces between the similar charges of MB molecules adsorbed on the surface of the MSS and the MB in the bulk solution [20].

As previously explained, the MSS was milled by a mortar to obtain the particle sizes (x) between 250 and 400 μm. The effect of these particle sizes on removal efficiency is also investigated in Fig. 6. The rate of

adsorption decreased by increasing MSS particle sizes, which can be related to the lower surface area of MSS available for the adsorption of MB molecules; however, the final MB removal efficiency after 150 min slightly decreased from about 95–91%.

3.2.3. Effect of MB concentration

The effect of initial MB concentration on the adsorption performance was studied at MSS dosage of 1.5 g/L at pH 7.0 (Fig. 7). The experimental data illustrated that the MB removal (%) decreased with an
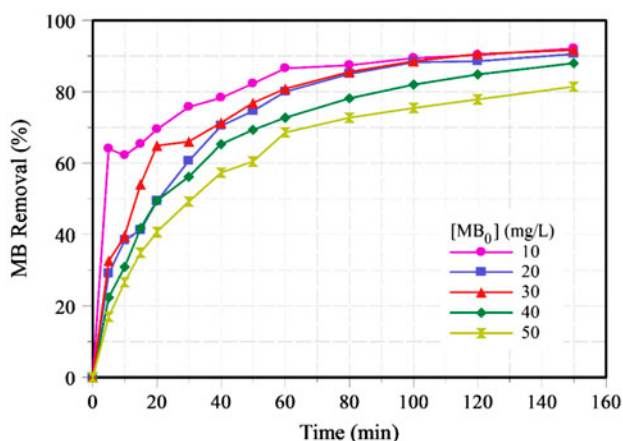
Fig. 7. Effect of initial dye concentration on MB removal (%) (MSS dosage: 1.5 g/L, pH 7.0, and *T*: 30℃).

increasing in the dye concentration. Increasing the concentration of MB from 10 to 30 mg/L does not have a significant effect on the removal efficiency after 150 min of adsorption, which can be related to the availability of adsorption sites on the surface of MSS to adsorb MB dye molecules in this range of concentration. But at higher concentrations of MB (up to 50 mg/L), the dye removal decreases from about 91 to 81%, which may be resulted from the saturation of the

adsorption sites by MB molecules, and also the repulsion forces between the adsorbed and bulk MB dye molecules [24,25].

3.2.4. Effect of salt

Various types of salts are employed as exhausting or retarding agents in textile processes, and their existence in textile wastewater is inevitable; hence, in this study, the MB removal (%) changes in the presence of various concentrations (0.01–0.15 M) of inorganic salts of different types are investigated and exhibited in Fig. 8. It can be seen that in all cases, the removal efficiencies decrease after the addition of salt to the solution. The salt molecules contain smaller cations (Na^+, K^+, and Ca^{2+}) rather than the cationic MB dye molecules. So, these small cations are rapidly adsorbed to the adsorbent, where they occupy the adsorption sites and consequently, prevent MB dye molecules in the bulk from moving toward the adsorbent by the repulsion forces [20,26].

3.2.5. Desorption and regeneration studies

The MB-loaded MSS was added to distilled water at various pH values to evaluate the desorption properties of the adsorbent. The results in Fig. 9
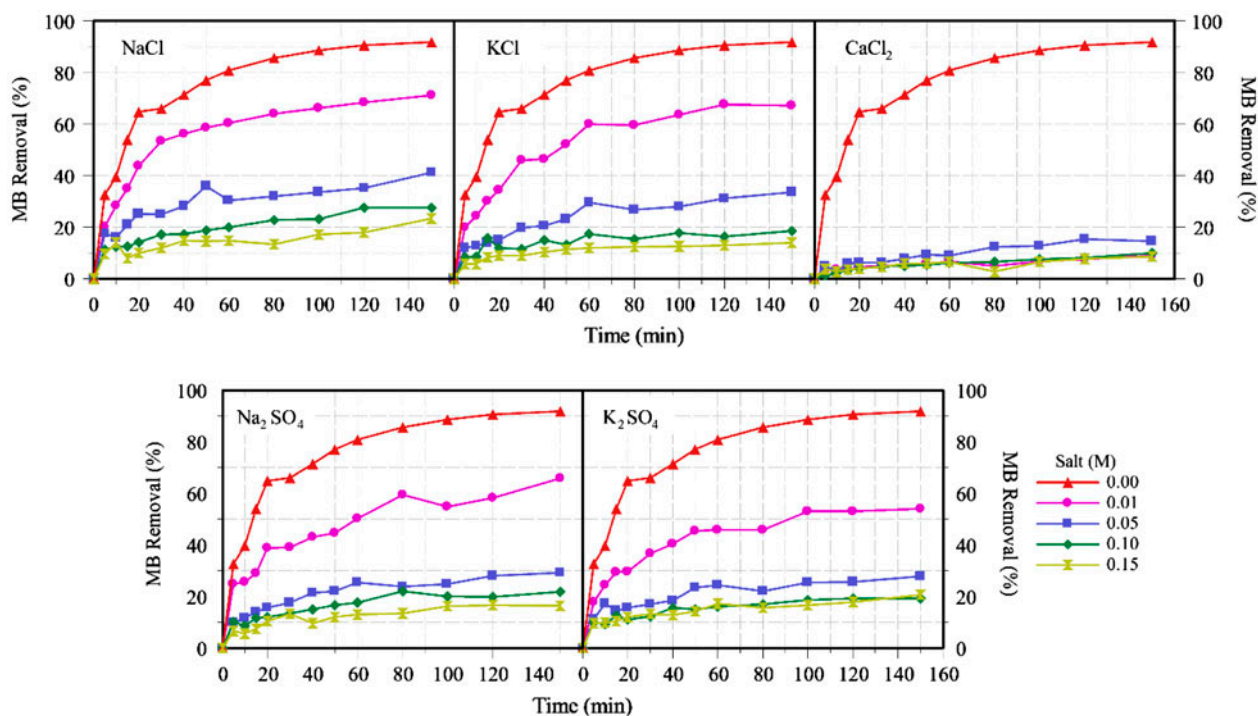
Fig. 8. Effect of inorganic salts on MB removal (%) ([MB_0]: 30 mg/L, MSS dosage: 1.5 g/L, pH 7, and *T*: 30℃).
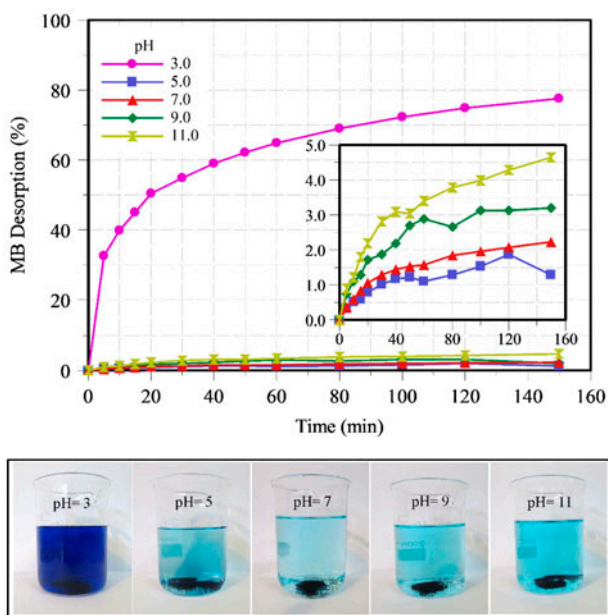
Fig. 9. Desorption (%) of MSS–MB at various pH values (MSS dosage: 0.8 g/L, and *T*: 30℃).

indicate that the highest desorption percent (77.5%) was obtained in acidic media at pH 3.0. The desorption (%) at higher pH values does not exceed 4.5% (Fig. 9, inner diagram). These results can be explained by the fact that at low pH values, the positively charged sites on the surface of the adsorbent increase by the protonation and facilitate desorption of positively charged MB molecules that had been adsorbed on MSS earlier [20,27].

The reusability and regeneration of MSS was evaluated for seven cycles of adsorption and desorption of MB dye molecules. The adsorption processes were carried out at pH 7.0, MB concentration of 30 mg/L, and MSS dosage of 1.5 g/L, which were

obtained as the optimum conditions for dye removal. Desorption procedures were performed at pH values of 1.0, 2.0, and 3.0 with the adsorbent dosage of 1.5 g/L. The results shown in Fig. 10 illustrate that the removal efficiencies of MB using MSS after six cycles are higher than 92% along with the desorption (%) of 57–71%. After the seventh cycle, the adsorption and desorption (%) decreased to 69 and 48%, respectively. The weight loss (%) of MSS was also calculated during these regeneration cycles and after seven cycles of adsorption and desorption, only 3% of weight loss was observed. According to these results, MSS has explored adequate regeneration properties as a natural adsorbent.

3.3. Equilibrium studies

3.3.1. Isotherm parameters

Three equilibrium isotherm models (Langmuir, Freundlich, and Temkin) were investigated to establish the appropriate correlations between the equilibrium data [28]. The homogeneous surface of the adsorbent with no interaction between its molecules, a non-uniform distribution of the heat of adsorption over the surface, and the linear reduction of heat of adsorption with the coverage due to the adsorbent–adsorbate interactions are the main assumptions of Langmuir, Freundlich, and Temkin isotherm equations, respectively [29].

The linear form of Langmuir, Freundlich, and Temkin isotherm equations (Eqs. ((4)–(6))) was employed for the removal of MB from MSS.

$$C_e/q_e = (1/K_L q_m) + (C_e/q_m) \tag{4}$$

$$\log q_e = \log K_F + (1/n) \log C_e \tag{5}$$
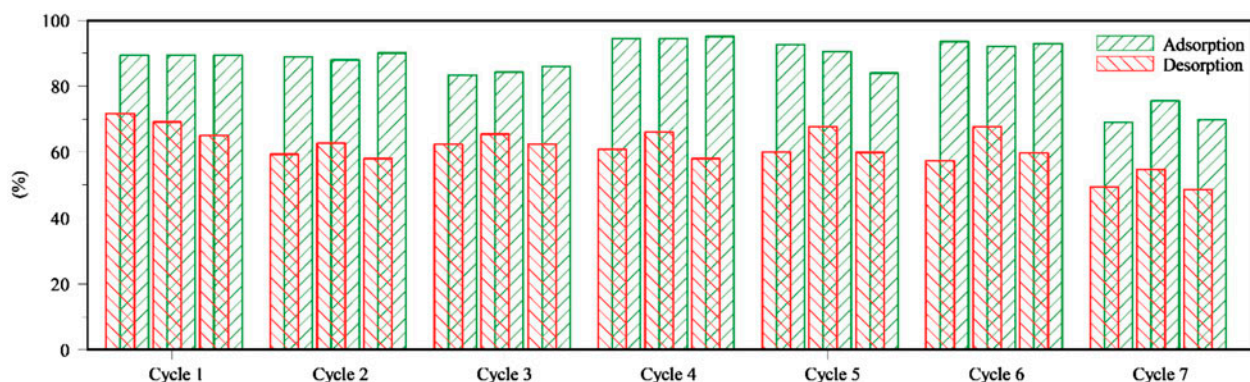
Fig. 10. Regeneration cycles for adsorption ([MB$_0$]: 30 mg/L, MSS dosage: 1.5 g/L, pH 7, and *T*: 30℃) and desorption (MSS dosage: 1.5 g/L, *T*: 30℃, and left: pH 1.0, middle: pH 2.0, and right: pH 3.0).

$$q_e = B_T \ln K_T + B_T \ln C_e \tag{6}$$

$$B_T = RT/b \tag{7}$$

where q_e is the concentration of MB on the adsorbent at equilibrium (mg/g), C_e is the equilibrium concentration of MB in solution (mg/L), and q_m is the maximum capacity of adsorbent (mg/g). K_L and K_F are the Langmuir and Freundlich constants, while B_T (Eq. (7)) and K_T are the Temkin constants [30]. Also, T is the absolute temperature (K) and R is the universal gas constant (8.314 J/(mol K)). The theoretical plots for each isotherm have been drawn for various initial MB concentrations and adsorbent dosages (data not shown), and the calculated isotherm parameters for the adsorption system are given in Table 1. The linear coefficient of determination (R^2, the variability in the dependent variable that has been explained by the regression line) and non-linear Chi-square (χ^2, sum of squares of the differences between the experimental and calculated data divided by the calculated data) are also represented in Table 1 as error functions to analyze the best fitted isotherm models to the experimental results. χ^2 can be written as Eq. (8):

$$\chi^2 = \sum \frac{(q_{e,exp} - q_{e,cal})^2}{q_{e,cal}} \tag{8}$$

where $q_{e,exp}$ and $q_{e,cal}$ are the experimental and calculated adsorption capacities (mg/g), respectively. High R^2 and low χ^2 values determine that an isotherm model is well fitted to the adsorption system. Our results in Table 1 demonstrate that high correlation coefficient values are obtained for both Langmuir and Temkin equations, but the considerably smaller Chi-square values are only achieved for the Temkin model. This means that the Temkin model can properly describe our adsorption experimental data [31,32]. Therefore, according to the assumption of Temkin isotherm model, the existing interaction between the MB dye molecules and MSS adsorbent will cause the heat of adsorption to vary linearly by the surface coverage of MB dye molecules on MSS.

3.3.2. Kinetic parameters

Several kinetic models including the pseudo-first-order, pseudo-second-order, and intraparticle diffusion models were examined to demonstrate the adsorption mechanism and rate constant [6]. The pseudo-first-order rate equation is written as Eq. (9) [33]:

$$\log(q_e - q_t) = \log(q_e) - (k_1/2.303)t \tag{9}$$

where q_e, q_t, and k_1 are the amounts of dye adsorbed (mg/g) at equilibrium and at any time, t (min), and the pseudo-first-order rate constant (1/min), respectively.

The pseudo-second-order kinetic model is also investigated employing the Eq. (10), where k_2 is the pseudo-second-order equilibrium rate constant (g/(mg min)) [34]:

$$t/q_t = 1/k_2 q_e^2 + (1/q_e)t \tag{10}$$

The slopes and intercepts of the plots of $\log(q_e - q_t)$ and t/q_t vs. t were used to calculate the rate constants, which are represented in Table 2 along with the experimental q_e, coefficients of determination (R^2), and calculated q_e values at different dye concentrations and adsorbent dosages. The values of correlation coefficients for different kinetic models demonstrated that the adsorption of MB by MSS had followed the pseudo-first-order kinetic model with the highest R^2 values. In addition, the experimental and calculated q_e values for the pseudo-first-order kinetic model were very close to each other.

In order to study the multilinearity of the adsorption process and investigate the diffusion mechanism, Eq. (11) is applied to the obtained data from the adsorption of MB [35]:

$$q_t = k_p t^{0.5} + I \tag{11}$$

Table 1
Isotherm parameters of adsorption of MB on MSS

	Langmuir				Freundlich				Temkin				
	q_m	K_L	R^2	χ^2	$\log K_F$	$1/n$	R^2	χ^2	K_T	B_T	b	R^2	χ^2
[MB]$_0$: 10–50 (mg/L)	34.72	0.23	0.977	45,770.085	2.053	0.58	0.916	1.824	2.095	133.02	18.91	0.956	0.383
[MSS]: 0.5–2.0 (g/L)	28.01	0.80	0.996	14,428.53	1.15	0.25	0.772	1.211	8.92	5.18	486.18	0.999	0.004

Table 2
Kinetic constants for MB adsorption on MSS

		Dye concentration (mg/L)				MSS dosage (g/L)			
		20	30	40	50	0.5	1.0	1.5	2.0
Pseudo-first-order	$(q_e)_{exp}$ (mg/g)	11.758	17.713	21.849	25.127	20.940	23.134	17.713	13.911
	$(q_e)_{cal}$ (mg/g)	10.960	13.996	19.588	25.663	19.688	18.836	13.996	11.746
	K_1 (1/min)	0.039	0.038	0.036	0.039	0.029	0.030	0.038	0.053
	R^2	0.991	0.976	0.995	0.981	0.718	0.985	0.976	0.987
Pseudo-second-order	$(q_e)_{cal}$ (mg/g)	13.038	18.904	24.272	28.986	25.510	24.752	18.904	14.749
	K_2 (g/(mg min))	0.005	0.005	0.003	0.002	0.001	0.003	0.005	0.010
	R^2	0.970	0.986	0.973	0.958	0.755	0.972	0.986	0.993
Intraparticle diffusion	K_p (mg/(g s$^{1/2}$))	1.193	1.708	2.245	2.668	1.999	2.232	1.708	1.305
	I	1.036	2.788	1.653	0.835	0.687	2.485	2.788	3.065
	R^2	0.969	0.918	0.965	0.979	0.780	0.964	0.918	0.880

where k_p (mmol/(g s)) refers to the intraparticle diffusion rate constant and I is the constant related to the thickness of the boundary layer. k_p, I, and R^2 were also calculated from the slopes and intercepts of the plots of q_t against $t^{0.5}$ at different MB and MSS concentrations (Table 2).

If the plots of q_t against $t^{0.5}$ are linear, then the intraparticle diffusion will be involved in the adsorption process, and if the lines pass through the origin, this mechanism will be the rate-controlling step. In the adsorption of MB by MSS, the lines do not pass through the origin (Fig. 11), which means that some level of boundary layer is involved in the removal process; and the intraparticle diffusion is not the only rate-limiting step and the adsorption can be controlled by other kinetic models [36].

3.3.3. Thermodynamic parameters

In here, the adsorption of MB on MSS was conducted at 303, 313, 323, and 333 K to study the thermodynamic parameters (Gibbs free energy (ΔG), enthalpy (ΔH), and entropy (ΔS)) of the adsorption process. These thermodynamic parameters are calculated according to Eqs. ((12)–(14)). The data are reported in Table 3 [37].

$$\Delta G = -RT \ln(q_e/C_e) \quad (12)$$

$$\ln(q_e/C_e) = (\Delta S/R) - (\Delta H/RT) \quad (13)$$

where q_e and C_e are the dye concentrations on MSS at equilibrium (mg/g) and in solution (mg/L), respectively, R is the universal gas constant (8.314 J/(mol K)), and T is the absolute temperature (K). The slope and intercept of the plot of $\ln (q_e/C_e)$ vs. $1/T$
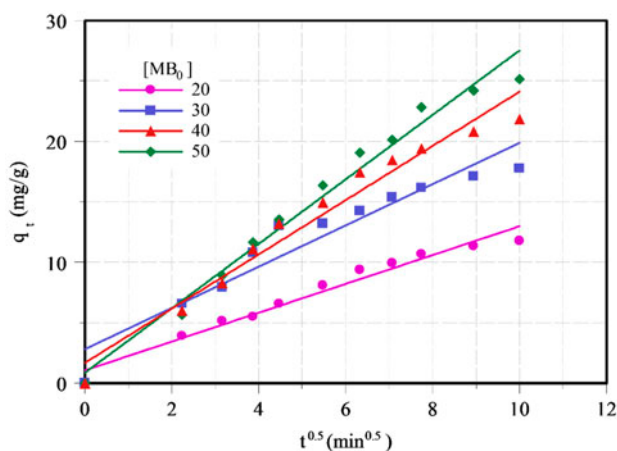
Fig. 11. Intraparticle diffusion plots for the adsorption of MB on MSS at various MB concentration (MSS dosage: 1.5 g/L, and T: 30℃).

Table 3
Thermodynamic parameters of adsorption of MB on MSS

T (K)	ΔG (kJ/mol)	ΔH (kJ/mol)	ΔS (kJ/mol K)
303	−4.04	9.44	0.045
313	−5.21		
323	−5.18		
333	−5.53		

resulted the ΔH and ΔS parameters and ΔG can be calculated using Eq. (14):

$$\Delta G = \Delta H - T\Delta S \quad (14)$$

The effect of temperature on MB removal efficiency indicated that the adsorption process was a spontaneous process confirmed by the negative values of ΔG.

Table 4
Experimental data for various adsorbent for the removal of MB

Adsorbent	C_0 (mg/L)	Adsorbent dosage (g/L)	pH	q_m (mg/g)	ΔS (kJ/mol K)	ΔH (kJ/mol)	Temp. (K)	Refs.
Arthrospira platensis	100	0.5	7.5	89.6	−0.011	−19.81	298	[39]
Untreated lignite	100	1.5	Natural	41.2	−0.186	58.19	333	[40]
Breadnut peel	100	2.0	6.0	409.1	64.57	−25.44	298	[41]
Almond gum	100	2	6.0	500.0	–	–	323.16	[42]
Yellow passion fruit peel	480	20	9.0	2.2	–	–	298	[43]
Date Palm Leaves	200	1.0	6.5	58.1	12.97	8.10	333	[44]
Platanus orientalis leaf	180	1.6	12.0	114.9	33.91	9.94	333	[45]
Melon seed shell	50	1.5	7.0	34.72	0.045	9.44	303	This study

On the other hand, the positive ΔH and ΔS values explore that the adsorption process is an endothermic reaction with increasing randomness at the solid/liquid interface during the removal process. Also, $-20 < \Delta G < 0$ and $-80 < \Delta G < 400$ kJ/mol refer to the physisorption and chemisorption processes; and the values obtained for the removal of MB by MSS are within the ranges of the physisorption mechanism [38].

3.4. Comparative study

The experimental results from several investigations employing low-cost adsorbents for the removal of MB are collected and summarized in Table 4. According to these data, the conditions applied for the adsorption processes and the considered values for operating parameters are different for each study. Wide ranges of initial dye concentration (50–480 mg/L), pH (6–12), and adsorbent dosage (0.5–20) have been examined, and therefore, the direct comparison of their final data (q_m) will not reveal the correct and accurate result. However, the promising results for the removal of MB by MSS in this research showed its adequate performance and efficiency at low concentrations of MB, compared to the other studies where the removal of MB is investigated at high concentrations, which leads to higher values of q_m.

4. Conclusion

In the present study, the removal of MB from simulated colored solutions was investigated using the natural and low-cost MSS as the adsorbent. The FESEM images and BET results showed the relatively porous surface of MSS, X-ray diffraction patterns confirmed the cellulosic nature of MSS, and the FTIR spectra confirmed the existence of C=O, C–O, C–H, and C≡C groups in the structure of MSS, which can be responsible for the adsorption of cationic MB dye

molecules at pH values above 5.5, at which the surface of MSS is negatively charged according to the obtained isoelectric pH. The effect of important parameters such as initial dye concentration, pH, and MSS dosage was studied on the adsorption efficiency. The experimental data showed that the addition and/or increasing the amount of inorganic salts to the solution have decreased the maximum accessible removal efficiency and lowered the adsorption performance. The regeneration studies of MSS explored its reusability for six cycles with removal efficiencies of >92% at acidic media. The investigation of equilibrium isotherm and kinetics at various MB concentrations and MSS dosages demonstrated that the adsorption process using MSS had followed the Temkin isotherm with high R^2 and low χ^2 values; and the pseudo-first-order kinetic model was best fitted to the experimental data. The thermodynamic parameters obtained by changing the solution temperatures illustrated that the adsorption was an endothermic ($\Delta H > 0$) and spontaneous ($\Delta G < 0$) process. The results explored that the natural and low-cost MSS could be employed as an efficient industrial waste for the effective removal of MB dye molecules from the polluted water streams.

References

[1] G. Crini, Non-conventional low-cost adsorbents for dye removal: A review, Bioresour. Technol. 97(9) (2006) 1061–1085.

[2] L. Cottet, C.A.P. Almeida, N. Naidek, M.F. Viante, M.C. Lopes, N.A. Debacher, Adsorption characteristics of montmorillonite clay modified with iron oxide with respect to Methylene Blue in aqueous media, Appl. Clay Sci. 95 (2014) 25–31.

[3] M. Roosta, M. Ghaedi, A. Daneshfar, R. Sahraei, A. Asghari, Optimization of the ultrasonic assisted removal of Methylene Blue by gold nanoparticles loaded on activated carbon using experimental design methodology, Ultrason. Sonochem. 21(1) (2014) 242–252.

[4] E. Pajootan, M. Arami, N.M. Mahmoodi, Binary system dye removal by electrocoagulation from synthetic and real colored wastewaters, J. Taiwan Inst. Chem. Eng. 43(2) (2012) 282–290.

[5] E. Pajootan, M. Arami, M. Rahimdokht, Application of carbon nanotubes coated electrodes and immobilized TiO$_2$ for dye degradation in a continuous photocatalytic-electro-fenton process, Ind. Eng. Chem. Res. 53 (42) (2014) 16261–16269.

[6] A.S. Özcan, A. Özcan, Adsorption of acid dyes from aqueous solutions onto acid-activated bentonite, J. Colloid Interface Sci. 276(1) (2004) 39–46.

[7] Q.H. Hu, S.Z. Qiao, F. Haghseresht, M.A. Wilson, G.Q. Lu, Adsorption study for removal of basic red dye using bentonite, Ind. Eng. Chem. Res. 45(2) (2005) 733–738.

[8] M.T. Yagub, T.K. Sen, S. Afroze, H.M. Ang, Dye and its removal from aqueous solution by adsorption: A review, Adv. Colloid Interface Sci. 209 (2014) 172–184.

[9] A. Ebrahimi, M. Arami, H. Bahrami, E. Pajootan, Fish bone as a low-cost adsorbent for dye removal from wastewater: Response surface methodology and classical method, Environ. Model. Assess. 18 (2013) 1–10.

[10] A. Ebrahimi, E. Pajootan, M. Arami, H. Bahrami, Optimization, kinetics, equilibrium, and thermodynamic investigation of cationic dye adsorption on the fish bone, Desalin. Water Treat. 53 (2013) 1–11.

[11] E. Daneshvar, M.S. Sohrabi, M. Kousha, A. Bhatnagar, B. Aliakbarian, A. Converti, A.-C. Norrström, Shrimp shell as an efficient bioadsorbent for Acid Blue 25 dye removal from aqueous solution, J. Taiwan Inst. Chem. Eng. 45(6) (2014) 2926–2934.

[12] V.S. Mane, P.V. Vijay Babu, Kinetic and equilibrium studies on the removal of Congo red from aqueous solution using Eucalyptus wood (*Eucalyptus globulus*) saw dust, J. Taiwan Inst. Chem. Eng. 44(1) (2013) 81–88.

[13] S. Karakaya, A. Kavas, S.N. El, N. Gündüç, L. Akdoğan, Nutritive value of a melon seed beverage, Food Chem. 52(2) (1995) 139–141.

[14] S.F.F. Ribeiro, A.P. Agizzio, O.L.T. Machado, A.G.C. Neves-Ferreira, M.A. Oliveira, K.V.S. Fernandes, A.O. Carvalho, J. Perales, V.M. Gomes, A new peptide of melon seeds which shows sequence homology with vicilin: Partial characterization and antifungal activity, Sci. Hortic. 111(4) (2007) 399–405.

[15] A. Verzera, G. Dima, G. Tripodi, C. Condurso, P. Crinò, D. Romano, A. Mazzaglia, C.M. Lanza, C. Restuccia, A. Paratore, Aroma and sensory quality of honeydew melon fruits (*Cucumis melo* L. subsp. melo var. inodorus H. Jacq.) in relation to different rootstocks, Sci. Hortic. 169 (2014) 118–124.

[16] L. Chen, Y.-H. Kang, J.-K. Suh, Roasting processed oriental melon (*Cucumis melo* L. var. makuwa Makino) seed influenced the triglyceride profile and the inhibitory potential against key enzymes relevant for hyperglycemia, Food Res. Int. 56 (2014) 236–242.

[17] N.S. Gill, M. Garg, R. Bansal, S. Sood, A. Muthuraman, M. Bali, P.D. Sharma, Evaluation of antioxidant and antiulcer potential of *Cucumis sativum* L. seed extract in rats, Asian, J. Clin. Nutr. 1 (2009) 131–138.

[18] C. Kannan, K. Muthuraja, M.R. Devi, Hazardous dyes removal from aqueous solution over mesoporous aluminophosphate with textural porosity by adsorption, J. Hazard. Mater. 244–245 (2013) 10–20.

[19] S.A. Kosa, G. Al-Zhrani, M. Abdel Salam, Removal of heavy metals from aqueous solutions by multi-walled carbon nanotubes modified with 8-hydroxyquinoline, Chem. Eng. J. 181–182 (2012) 159–168.

[20] L. Eskandarian, E. Pajootan, M. Arami, Novel super adsorbent molecules, carbon nanotubes modified by dendrimer miniature structure, for the removal of trace organic dyes, Ind. Eng. Chem. Res. 53(38) (2014) 14841–14853.

[21] S. Marković, A. Stanković, Z. Lopičić, S. Lazarević, M. Stojanović, D. Uskoković, Application of raw peach shell particles for removal of Methylene Blue, J. Environ. Chem. Eng. 3(2) (2015) 716–724.

[22] L. Eskandarian, M. Arami, E. Pajootan, Evaluation of adsorption characteristics of multiwalled carbon nanotubes modified by a poly(propylene imine) dendrimer in single and multiple dye solutions: Isotherms, kinetics, and thermodynamics, J. Chem. Eng. Data 59(2) (2014) 444–454.

[23] M. Ghaedi, M. Montazerozohori, M.N. Biyareh, K. Mortazavi, M. Soylak, Chemically bonded multiwalled carbon nanotubes as efficient material for solid phase extraction of some metal ions in food samples, Int. J. Environ. Anal. Chem. 93(5) (2012) 528–542.

[24] Z. Chen, J. Zhang, J. Fu, M. Wang, X. Wang, R. Han, Q. Xu, Adsorption of Methylene Blue onto poly(cyclotriphosphazene-co-4,4´-sulfonyldiphenol) nanotubes: Kinetics, isotherm and thermodynamics analysis, J. Hazard. Mater. 273 (2014) 263–271.

[25] M. Roosta, M. Ghaedi, A. Daneshfar, S. Darafarin, R. Sahraei, M.K. Purkait, Simultaneous ultrasound-assisted removal of sunset yellow and erythrosine by ZnS: Ni nanoparticles loaded on activated carbon: Optimization by central composite design, Ultrason. Sonochem. 21(4) (2014) 1441–1450.

[26] M. Muthukumar, N. Selvakumar, Studies on the effect of inorganic salts on decolouration of acid dye effluents by ozonation, Dyes Pigm. 62(3) (2004) 221–228.

[27] H. El Boujaady, M. Mourabet, M. Bennani-Ziatni, A. Taitai, Adsorption/desorption of Direct Yellow 28 on apatitic phosphate: Mechanism, kinetic and thermodynamic studies, J. Assoc. Arab Universities Basic Appl. Sci. 16 (2014) 64–73.

[28] A. Öztürk, E. Malkoc, Adsorptive potential of cationic Basic Yellow 2 (BY2) dye onto natural untreated clay (NUC) from aqueous phase: Mass transfer analysis, kinetic and equilibrium profile, Appl. Surf. Sci. 299 (2014) 105–115.

[29] L. Eskandarian, M. Arami, E. Pajootan, Evaluation of adsorption characteristics of multiwalled carbon nanotubes modified by a poly(propylene imine) dendrimer in single and multiple dye solutions: Isotherms, kinetics, and thermodynamics, J. Chem. Eng. Data 59(2) (2014) 444–454.

[30] T. Madrakian, A. Afkhami, M. Ahmadi, H. Bagheri, Removal of some cationic dyes from aqueous solutions using magnetic-modified multi-walled carbon nanotubes, J. Hazard. Mater. 196 (2011) 109–114.

[31] Y.-S. Ho, A.E. Ofomaja, Kinetics and thermodynamics of lead ion sorption on palm kernel fibre from aqueous solution, Proc. Biochem. 40(11) (2005) 3455–3461.

[32] M. Ghaedi, A. Ansari, M.H. Habibi, A.R. Asghari, Removal of malachite green from aqueous solution by

zinc oxide nanoparticle loaded on activated carbon: Kinetics and isotherm study, J. Ind. Eng. Chem. 20(1) (2014) 17–28.

[33] W.-N.L. Siew-Teng Ong, P.-S. Keng, S.-L. Lee, Y.-T. Hung, S.-T. Ha, Equilibrium studies and kinetics mechanism for the removal of basic and reactive dyes in both single and binary systems using EDTA modified rice husk, Int. J. Phys. Sci. 5(5) (2010) 582–595.

[34] J. Gong, T. Liu, X. Wang, X. Hu, L. Zhang, Efficient removal of heavy metal ions from aqueous systems with the assembly of anisotropic layered double hydroxide Nanocrystals@carbon nanosphere, Environ. Sci. Technol. 45(14) (2011) 6181–6187.

[35] A. Roy, S. Chakraborty, S.P. Kundu, B. Adhikari, S.B. Majumder, Adsorption of anionic-azo dye from aqueous solution by lignocellulose-biomass jute fiber: Equilibrium, kinetics, and thermodynamics study, Ind. Eng. Chem. Res. 51(37) (2012) 12095–12106.

[36] A. Özcan, A.S. Özcan, Adsorption of Acid Red 57 from aqueous solutions onto surfactant-modified sepiolite, J. Hazard. Mater. 125(1–3) (2005) 252–259.

[37] H.Y. Zhu, R. Jiang, L. Xiao, G.M. Zeng, Preparation, characterization, adsorption kinetics and thermodynamics of novel magnetic chitosan enwrapping nano-sized γ-Fe₂O₃ and multi-walled carbon nanotubes with enhanced adsorption properties for methyl orange, Bioresour. Technol. 101(14) (2010) 5063–5069.

[38] M. Abdel Salam, M.A. Gabal, A.Y. Obaid, Preparation and characterization of magnetic multi-walled carbon nanotubes/ferrite nanocomposite and its application for the removal of aniline from aqueous solution, Synth. Met. 161(23–24) (2012) 2651–2658.

[39] D. Mitrogiannis, G. Markou, A. Çelekli, H. Bozkurt, Biosorption of Methylene Blue onto *Arthrospira platensis* biomass: Kinetic, equilibrium and thermodynamic studies, J. Environ. Chem. Eng. 3(2) (2015) 670–680.

[40] A. Gürses, A. Hassani, M. Kıranşan, Ö. Açışlı, S. Karaca, Removal of Methylene Blue from aqueous solution using by untreated lignite as potential low-cost adsorbent: Kinetic, thermodynamic and equilibrium approach, J. Water Proc. Eng. 2 (2014) 10–21.

[41] L.B.L. Lim, N. Priyantha, D.T.B. Tennakoon, H.I. Chieng, M.K. Dahri, M. Suklueng, Breadnut peel as a highly effective low-cost biosorbent for Methylene Blue: Equilibrium, thermodynamic and kinetic studies, Arabian J. Chem. (in press), doi: 10.1016/j.arabjc.2013.12.018.

[42] F. Bouaziz, M. Koubaa, F. Kallel, F. Chaari, D. Driss, R.E. Ghorbel, S.E. Chaabouni, Efficiency of almond gum as a low-cost adsorbent for Methylene Blue dye removal from aqueous solutions, Ind. Crops Prod. 74 (2015) 903–911.

[43] F.A. Pavan, A.C. Mazzocato, Y. Gushikem, Removal of Methylene Blue dye from aqueous solutions by adsorption using yellow passion fruit peel as adsorbent, Bioresour. Technol. 99(8) (2008) 3162–3165.

[44] M. Gouamid, M.R. Ouahrani, M.B. Bensaci, Adsorption equilibrium, kinetics and thermodynamics of Methylene Blue from aqueous solutions using date palm leaves, Energy Procedia 36 (2013) 898–907.

[45] M. Peydayesh, A. Rahbar-Kelishami, Adsorption of Methylene Blue onto *Platanus orientalis* leaf powder: Kinetic, equilibrium and thermodynamic studies, J. Ind. Eng. Chem. 21 (2015) 1014–1019.